Application of Momentum Coupled Muon Scattering Tomography in Estimating Special Nuclear Materials

Authors: Chen, Dr. Ziyang, Liu, Dr. Jianing, Liu, Daming, Gong, Hui, Li, Dr. Yulei, Prof. Yi Wang, Han, Ms. Dong, Guo, Baohong, Prof. Yi Wang

Date: 2025-11-17T00:00:00+00:00

Abstract

Muon scattering tomography has emerged as a prominent research direction in recent years, showing great potential in various applications such as cargo inspection and nuclear material detection. An increasing number of studies have highlighted the critical importance of incorporating muon momentum information, which can be obtained by Time of Flight (ToF) system as an alternative, to enhance image quality and rapid inspection capability in muon scattering tomography. MRPC (Multi-gap Resistive Plate Chamber) detectors are characterized by excellent time resolution and are widely used in ToF systems. Our recent research shows the time resolution of very narrow gaps MRPC reaching 16 ps and the spatial resolution of sealed MRPC achieving 0.5 mm. Therefore, MRPC holds great potential in muon scattering tomography. In this work, we employ Geant4 toolkit to simulate a realistic and detailed muon scattering tomography system consisting of MRPC-ToF and MRPC trajectory detection modules to estimate the internal structure of the classical Steve Fetter hypothetical model. The results indicate that momentum information significantly contributes to improving the quality of muon scattering tomography. To further improve imaging performance, a specialized neural network U-Net is applied to the reconstructed images to extract nuclear material regions, thereby enhancing the effectiveness and resolution of muon scattering tomography.

Full Text

Preamble

Application of Momentum Coupled Muon Scattering Tomography in Estimating Special Nuclear Materials

Zi-Yang Chen,[1] Jia-Ning Liu,[2] Da-Ming Liu,[1] Yu-Lei Li,[2] Hui Gong,[1] Yi Wang,[1],* Dong Han,[1] and Bao-hong Guo[1]
[1]Department of Engineering Physics, Tsinghua University, Beijing 100084, China
[2]China Institute of Nuclear Industry Strategy, CINIS, No. 43, FuCheng Road, 100048, Beijing, China

Muon scattering tomography has emerged as a prominent research direction in recent years, showing great potential in various applications such as cargo inspection and nuclear material detection. An increasing number of studies have highlighted the critical importance of incorporating muon momentum information, which can be obtained by Time of Flight (ToF) systems as an alternative approach, to enhance image quality and rapid inspection capability in muon scattering tomography. MRPC (Multi-gap Resistive Plate Chamber) detectors are characterized by excellent time resolution and are widely used in ToF systems. Our recent research shows the time resolution of very narrow gap MRPC reaching 16 ps and the spatial resolution of sealed MRPC achieving 0.5 mm. Therefore, MRPC holds great potential for muon scattering tomography applications.

In this work, we employ the Geant4 toolkit to simulate a realistic and detailed muon scattering tomography system consisting of MRPC-ToF and MRPC trajectory detection modules to estimate the internal structure of the classical Steve Fetter hypothetical model. The results indicate that momentum information significantly contributes to improving the quality of muon scattering tomography. To further improve imaging performance, a specialized neural network U-Net is applied to the reconstructed images to extract nuclear material regions, thereby enhancing the effectiveness and resolution of muon scattering tomography.

Keywords: Muon Scattering Tomography, MRPC, Time of Flight, Geant4, U-Net

Introduction

Muon scattering tomography (MST) has been rapidly developing in the nuclear technology field [**?**]. By exploiting naturally generated cosmic-ray muons and the fact that muon scattering angles are sensitive to the atomic number of the material traversed, MST enables internal structure detection or imaging of objects under investigation without artificial radioactive sources and without causing radiation damage. At present, MST can be applied in border security [**?**], such as suspicious goods inspection in cargo containers [**?**, **?**]. MST can also be applied in the management of nuclear fuel and waste [**?**, **?**], as well as reactor imaging [**?**, **?**] and industrial sector applications [**?**]. Depending on different applications and requirements, muon scattering imaging technology can be divided into two main development directions: the first focuses on rapid detection capability [**?**, **?**], where muon information collected within a relatively

short exposure time is analyzed to quickly determine the presence or absence of target materials, though this approach cannot provide direct MST images; the second focuses on fine imaging capability [**?**], aimed at producing high-quality images of the internal structure of objects.

Regardless of whether for rapid detection or detailed imaging, growing evidence shows that muon momentum information is critical for enhancing the performance of muon scattering tomography systems [**?**, **?**]. Worldwide, various approaches have been explored for estimating muon momentum within MST systems. Some studies introduce extra scattering materials into the system, analyzing the degree of muon scattering in these media to infer momentum [**?**]; others exploit the energy sensitivity of Cherenkov detectors, employing multilayer Cherenkov detectors to classify muon momentum [**?**]. In our previous work [**?**], we proposed incorporating a Time of Flight (ToF) system into the MST system to measure and calculate muon momenta, focusing on improving the system' s rapid detection capability for special nuclear materials.

In the field of MST, multiple detector technologies have been employed for muon trajectory measurement, including scintillation detectors [**?**], drift tubes [**?**], RPCs [**?**] and MRPCs. Among them, MRPCs (Multi-gap Resistive Plate Chambers) [**?**] are outstanding gas detectors, offering high efficiency for charged particle detection, excellent position resolution and orthogonal readout capability, making them an excellent choice for muon detection. Moreover, MRPCs are renowned for their ultrahigh time resolution [**?**] and have been widely used in high-energy physics experiments [**?**].

Based on our earlier work, we improved the system design and developed a Multi-functional Cosmic Ray Imaging System (MCRIS) composed entirely of MRPC detectors, with efficacious capability of momentum measurement. The main content of this paper is the detailed construction of a simulated MCRIS system using the Geant4 toolkit [**?**], followed by an in-depth investigation of its imaging performance for a specific nuclear device: the hypothetical nuclear device model proposed by Professor Steve Fetter, an expert in nuclear arms control and nonproliferation. Our study demonstrates the importance and necessity of incorporating momentum information in MST, and further employs a U-Net algorithm to optimize the imaging results, extracting the structural features of interest while reducing muon exposure time.

[FIGURE:1] Conceptional Structure of MCRIS.

II. METHODS

A. Principle of Muon Scattering Tomography

Cosmic-ray muons, with an average energy of about 4 GeV, are generally regarded as minimum ionizing particles. After passing through matter, muons undergo multiple Coulomb scattering (MCS). The distribution of the multiple

scattering angles is strongly correlated with the atomic number Z of the material along the muon path. This relationship is expressed in Equation (1) [**?**]:

$$\theta_0 = \frac{13.6\text{MeV}}{p\beta c}\sqrt{\frac{L}{L_{rad}}}\left[1 + 0.038\ln\left(\frac{L}{L_{rad}}\right)\right]$$

Based on our previous work [**?**], we introduced the concepts of the nominal muon scattering angle θ_{nom} and the nominal scattering density per unit path length λ_{nom}. The nominal muon scattering angle is defined by the following expression:

$$\theta_{nom} = \theta_i \frac{p_i}{p_0}$$

In Equation (2), θ_i, p_i, L_i represent respectively the scattering angle, momentum and traversed path length of a certain muon. The significance of θ_{nom} and λ_{nom} is that λ_{nom} accounts for the effects of the incident muon momentum and muon path, thereby ensuring that the nominal scattering density per unit path length, which is directly related to the material' s scattering length L_{rad}, depends solely on the distribution of the nominal muon scattering angles in Equation (3), where p_0 is a constant:

$$\lambda_{nom} = \sum \theta_{nom} \propto \frac{1}{L_{rad}}$$

In other words, the distribution of θ_{nom} of muons directly reflects L_{rad}, or atomic number Z of objects under investigation.

B. Simulation in Geant4

In Geant4 simulation, two types of MRPC detector systems are modeled: a high position resolution MRPC (named Hp_{MRPC}) system and a high time resolution MRPC (named Ht_{MRPC}) system. The Hp_{MRPC} system consists of two modules, each composed of three MRPCs for muon track reconstruction, while the Ht_{MRPC} system contains two Ht_{MRPCs} in total. Both detector types were constructed in Geant4 following the actual experimental configuration.

Specifically, each Ht_{MRPC} comprises four chambers with 32 gas gaps, where each gap has a thickness of 0.128 mm and the glass plates are 0.4 mm thick. Each Hp_{MRPC} consists of a single chamber with five gas gaps of 0.25 mm and glass plates of 0.7 mm. For both detector types, the PCB thickness is 1 mm; the Mylar layer is 0.5 mm; and the honeycomb support panel is 10 mm, all consistent with the experimentally measured specifications.

To better match experimental performance, the two MRPC types are calibrated using the measured spatial and temporal resolutions described in the literature. For the Hp_{MRPC}, a spatial resolution of 0.5 mm (close to 0.404 mm in [**?**]) is applied. The muon hit position is determined by averaging the ionization electrons' positions across all gas gaps, with additional Gaussian smearing (σ = 0.5 mm, $\mu = 0$) independently applied to the x and y coordinates (we suppose the z coordinate is along the vertical direction in reality). For the Ht_{MRPC}, a time resolution of 20 ps (close to 16.7 ps in [**?**]) is assumed. The muon arrival time is obtained by averaging the ionization times of the primary charges across all gaps then adding a Gaussian fluctuation with $\sigma = 20$ ps and $\mu = 0$.

In this work, the object for MST is based on the hypothetical nuclear device model proposed by Steve Fetter. Its structural configuration is shown in Fig. 2 [FIGURE:2], consisting of an outer aluminum casing (blue), a surrounding explosive layer (lightest gray), a uranium tamper (darkest gray), a beryllium reflector (gray), and a fissile core (red), all enclosed within a lead container (not shown in Fig 2). In this work, the fissile core material is selected as WgU, with a corresponding thickness of 1.23 cm and an outer diameter of 7 cm. The thicknesses of other material layers are kept consistent with those shown in Fig. 2.

The geometrical arrangement of the Hp_{MRPC} and Ht_{MRPC} systems is illustrated in Fig. 3 [FIGURE:3]. In the MCRIS, the two Ht_{MRPC} detectors are placed at the top and bottom positions to determine the nominal muon scattering angles, while the Fetter model is positioned between the two Hp_{MRPC} modules. The aim is not only to identify any displacement of the Fetter model inside the container but to further reconstruct its internal structure utilizing MST.

C. U-Net

U-Net is a convolutional neural network (CNN) architecture originally proposed for biomedical image segmentation [**?**]. It follows an encoder-decoder structure (Fig. 4 [FIGURE:4]) where the encoder (contracting path) progressively captures contextual information through convolution and pooling operations, while the decoder (expanding path) performs upsampling and concatenates feature maps from corresponding encoder layers via skip connections. This symmetric "U-shaped" design enables the network to combine high-level semantic information with fine-grained spatial details, leading to precise localization and accurate boundary reconstruction. Meanwhile, U-Net is particularly well suited for scenarios involving small datasets [**?**]. Owing to its efficiency and strong generalization ability, U-Net and its variants have been widely applied not only in medical imaging but also in diverse fields such as remote sensing, materials science, and particle detector data analysis.

In this work, the U-Net is primarily utilized to segment regions of high-Z materials based on the MST results of the Fetter model. Our U-Net follows a symmet-

ric encoder-decoder design with four downsampling and four upsampling stages, connected through skip connections to preserve spatial information. The network takes grayscale images as input and produces a single-channel segmentation map that highlights the high-Z structures of interest from MST reconstructions.

III. ANALYSIS AND RESULTS

A. Evaluation of Momentum Resolution and Realistic Energy Loss Effects

According to Equation (2), the nominal scattering angle θ_{nom} encapsulates several key physical quantities, including the actual scattering angle θ_i, the incident muon momentum p_i and the effective material thickness traversed by the muon L_i. Since p_i and L_i are difficult to measure directly, the method proposed in our previous work is adopted, in which estimated momentum $\hat{p}$ and estimated length of flight $\hat{L}_{flight}$ are employed instead. The principle for obtaining these estimated physical quantities is as shown in Equation (4) and (5):

$$\hat{L}_{flight} = \frac{H}{\cos(\theta_{zen})}$$

$$\hat{p} = \frac{m_\mu \hat{L}_{flight}}{\hat{t}_{flight}} \frac{1}{\sqrt{1 - \left(\frac{\hat{L}_{flight}}{\hat{t}_{flight} c}\right)^2}}$$

where H is the width of the tomography target; θ_{zen} is the incident zenith angle of a single muon; the estimated $\hat{t}_{flight}$ is obtained from the difference in arrival times measured by the two Ht-MRPC detectors. This approach has been validated in our previous work, though its accuracy is primarily confined to the low-energy muon regime [**?**].

However, a crucial consideration arises here: during propagation, muons continuously interact with the material, undergoing both MCS and ionization which causes energy loss simultaneously. For the Fetter model, muons with momenta below approximately 3 GeV/c are distinctly affected by these processes (Fig. 5 [FIGURE:5]), which must be carefully accounted for in the subsequent analysis.

In Fig. 5, the left panel compares the momentum spectra of all incident muons (those reaching the Fetter model) with those of the effective muons (i.e., muons successfully reaching the lower track module). A clear ionization energy loss effect induced by the target object can be observed: muons below a certain energy threshold fail to emerge from the object and therefore cannot contribute as valid events. The right panel shows the comparison between the incident and emitted momentum distributions of the effective muons, which can be approximately regarded as a shift of the incident spectrum toward lower energies. This

demonstrates that ionization energy loss cannot be neglected, particularly for low-momentum muons, which are the main focus of the ToF-based momentum measurement.

Ionization causes energy loss and, correspondingly, the muon's velocity to gradually decrease along its path. While this effect could be negligible for high-energy muons, it becomes nontrivial for muons below and around approximately 1 GeV, leading to a measurable reduction in velocity. Consequently, the velocity obtained from the ToF measurement represents the average velocity along the trajectory rather than the true incident velocity. This discrepancy introduces an inevitable bias in the calculation of the nominal scattering strength.

Therefore, before performing the displacement detection and internal structure imaging of the target Fetter model, a detailed evaluation and calibration of the momentum measurement accuracy are conducted. In this work, we analyze the correlation between the true incident momentum of muons before entering the Fetter model and the momentum reconstructed using the ToF method. The results show a clear positive correlation between the two, confirming the overall reliability of the TOF-based momentum estimation despite the aforementioned energy loss effects.

As shown in Fig. 6 [FIGURE:6], a clear positive correlation is observed between the momentum measured by the ToF method and the real incident momentum for muons with relatively low momenta, confirming the reliability and feasibility of the ToF-based momentum measurement (i.e., MCRIS). Furthermore, the correlations between true incident momentum and both the mean value and uncertainty of the measured momentum are quantitatively considered, as presented in Fig. 7

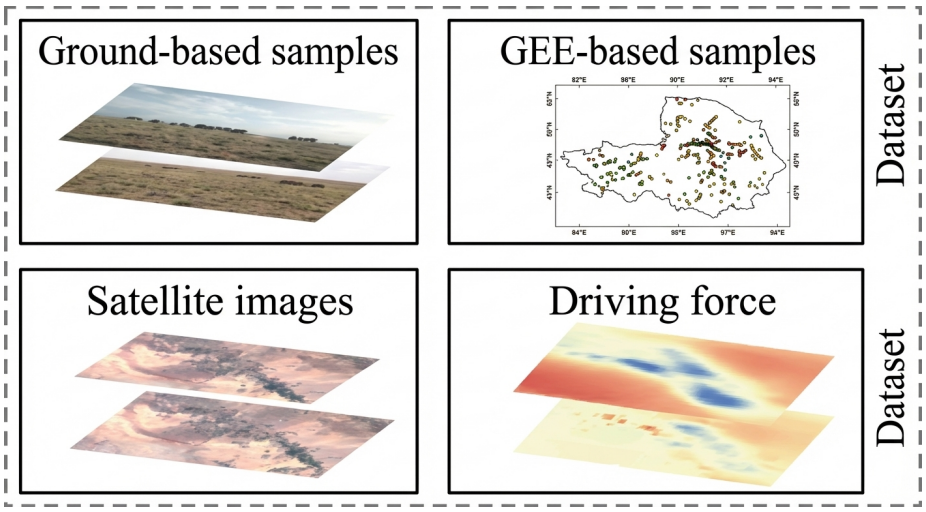

Figure 1: Figure 7

, where the blue and red curves represent the polynomial fitting results. In this work, the fitted correlations are utilized to infer the incident momentum of muons from the estimated values and to obtain the associated measurement uncertainty. This procedure effectively mitigates the influence of ionization energy loss on the ToF-based momentum determination, thus enhancing the imaging precision.

In the subsequent image reconstruction, MST images are reconstructed and obtained using the Point of Closest Approach (PoCA) algorithm.

B. Short-term Displacement Detection

For certain special nuclear materials or facilities (such as the Fetter model), it is important to determine whether the core components have experienced any displacement within the container during transportation or long-term storage. This is crucial both for safety assessment and for verifying the structural integrity and reliability of the container design. The proposed MCRIS system provides a rapid, non-intrusive inspection approach that allows the detection of small displacements of nuclear components without opening the container. It can also serve as a long-term monitoring tool, capable of identifying and warning of even minor positional changes within a short response time.

In this work, muon scattering tomography was conducted with the Fetter model positioned either at the center of the container or displaced by 1 cm, 3 cm, or 5 cm along some horizontal direction (named the x-axis in the analysis) from the center. Considering that the muon exposure time in this part is relatively short, the pixel size is set to 1 cm in order to ensure a sufficient number of muons within each PoCA pixel.

A 10-minute muon exposure is chosen as a representative short-term acquisition. Figure 8 [FIGURE:8] shows the corresponding muon scattering tomographic results: the upper panel illustrates the reconstruction based solely on the scattering angle, representing the conventional MST approach, while the lower panel presents the result obtained by incorporating MRPC-ToF estimated momentum information. For the Fetter model, such a short exposure is insufficient to reconstruct the overall structure, particularly the outer explosive layer, which remains almost indistinguishable, while the more internal structures containing heavy nuclear materials can still be discerned with reasonable clarity. A comparison between the two reconstruction approaches reveals that using only angular information produces a blurred depiction of the dense core, which is also highly sensitive to occasional large-angle scattering within single pixels. By contrast, inclusion of the momentum information markedly sharpens the outline of the heavy nuclear component and substantially improves the image contrast.

In addition, we compare the distribution of the 'PoCA centroid' along the x-axis obtained under shorter muon exposure times with the Fetter model positioned at the center of the container. Fig. 9 [FIGURE:9] illustrates the reconstructed results obtained under 1-min and 2-min muon exposure times (in such a short

period, attaining a high-quality MST image is challenging). The results show that, when the muon momentum information is not used, the 'PoCA centroid' distribution exhibits larger dispersion, whereas the inclusion of momentum information leads to a more concentrated distribution. Building upon this result, the approach introduced in our previous study can be applied to quantify the minimum detectable displacement and the corresponding detection time at a given confidence level, which may be the focus of future work.

C. Reconstructed Internal Structure of Fetter Model

To investigate the internal structure of the Fetter model, a long-term muon exposure simulation is performed, and the corresponding images are reconstructed. The results obtained under different data analysis methods are shown in Fig. 10 [FIGURE:10].

In Fig. 10, from left to right, we process the same set of muon scattering angle data, while only the treatment of the momentum information differs. Subfigure (a) shows the image reconstructed using only the scattering angle information, whereas subfigure (b) presents the result obtained by applying momentum obtained by ToF methods to all scattering angle data. A clear comparison between the two reveals that, without incorporating momentum information, the internal high-Z structure of the Fetter model cannot be effectively distinguished within the same muon exposure time. By contrast, when momentum information is included, a distinct "multi-ring" image of the Fetter model emerges: the innermost dark ring corresponds to the fissile core and the outer dark ring represents the tamper region, while the explosive layer remains barely distinguishable.

Considering the characteristics of the ToF-based momentum estimation, the uncertainty of the estimated momentum increases with increasing muon momentum. Therefore, for high-energy muons, the ToF method inevitably introduces larger errors. Following the approach adopted in our previous work, the applicable range of the ToF method is restricted to an artificially defined 'low-momentum region' and different treatment methods are applied to muons outside of this range. So according to the same logic, the maximum acceptable momentum-estimation uncertainty is also set to 60% as in prior considerations, which corresponds to a muon momentum of approximately 1 GeV/c. Thus, in our analysis, muons with estimated momenta below 1 GeV/c are defined as belonging to the 'low-momentum region' in this work.

Subfigure (c) shows the result obtained after excluding all muons outside the low-momentum region and performing MST imaging employing only the remaining data. In this case, the circular outline of the explosive layer (light pink in Fig. 10) becomes more discernible, and the rings corresponding to the internal high-Z materials appear more compact and well defined. However, in nuclear-related fields, using fewer data leads to larger statistical uncertainty; simply discarding low-momentum muons causes waste. To take advantage of these muons, their energy spectrum is analyzed to obtain the momentum mean value as well as

uncertainty within this range. According to this logic, the final result, shown in subfigure (d), clearly resolves the circular ring of the explosive layer while also providing enhanced contrast for the fissile core and tamper regions.

Figure 11 [FIGURE:11] presents a comparison between the final MST result of the Fetter model and its corresponding geometric model in Geant4. It can be observed that the relative positions of the explosive layer, tamper layer and Be reflective layer are generally consistent from the outside to the inside, whereas the thickness of the central fissile core shows a noticeable discrepancy.

For the fissile core, since it contains an internal hollow cavity, muons theoretically do not undergo MCS within this region. However, according to the principle of the PoCA algorithm, the MCS occurring along the entire muon trajectory are treated as a single equivalent scattering at the PoCA point. Therefore, a muon whose reconstructed PoCA point is inside the cavity has already traversed the entire Fetter model and experienced significant scattering. Moreover, due to the large variation in muon' s incident angles, the effective path lengths through different materials vary substantially among muons, even if their reconstructed PoCA points may be located at similar positions. The current PoCA reconstruction does not account for these influences, which leads to blurred or ill-defined edges in the reconstructed image.

This analysis further highlights the necessity of developing improved reconstruction algorithms that are better suited for complex multilayer structures such as the Fetter model.

D. Optimization Results Based on U-Net

The images shown in Figures 10 and 11 are obtained within a muon exposure time of about 200 hours. The detection efficiency of the detector for cosmic-ray muons is approximately 30.4%. Fig. 12 [FIGURE:12] shows several reconstructed results obtained within a maximum exposure time of 4,000 minutes. It can be observed that, with momentum information incorporated, the image quality at 4,000 minutes surpasses that of the 200-hour reconstruction without estimated momenta. This further demonstrates the essential role of muon momentum information in improving the accuracy and clarity of muon scattering imaging.

However, even with the inclusion of momentum information, the reconstruction at 4,000 minutes only weakly suggests the existence of the tamper layer. If we aim to obtain the internal structure of the target object (e.g., the Fetter model) within a shorter acquisition time, using only momentum information is not sufficient; advanced image processing algorithms are also required. Among image-processing algorithms, the U-Net architecture is particularly suitable for extracting regions of interest from images. For the Fetter model, the main regions of interest are the internal high-Z materials, i.e., the tamper and fissile core.

Prior to training the U-Net model, the reconstructed MST images undergo pre-processing, including Gaussian smoothing and a tailored windowing operation. The latter is inspired by windowing methods commonly used in the CT field, where adjusting the window width and level improves the contrast of target structures [**?**].

To enhance the generalization capability of the U-Net model, we generate additional training samples by modifying the layer thicknesses of the tamper and fissile core in Geant4. Two variant geometries are constructed, referred to as Fetter_{Variant1} and Fetter_{Variant2}. In Fetter_{Variant1}, the fissile core has a thickness of 2.23 cm and an outer diameter of 8 cm, while the tamper thickness is set to 2 cm. In Fetter_{Variant2}, the fissile core thickness is fixed at 1.23 cm with an outer diameter of 8 cm, and the tamper thickness is 3 cm. All other parameters remain identical to those of the original Fetter model.

The MST images under different muon exposure times are pre-processed in the same manner, after which the images are labeled and divided into training and test sets. These datasets are subsequently used to train the U-Net model, yielding the results shown in Fig. 13 [FIGURE:13] and 14:

For the original Fetter model, approximately 2,000 minutes of muon exposure are sufficient for the U-Net to extract the high-Z features of interest. In contrast, the two geometric variants require longer exposure times because their representation in the training dataset is smaller compared with the basic Fetter model. Consequently, the U-Net needs more data to accurately learn and reconstruct their high-Z structures. Nevertheless, these results demonstrate that incorporating a U-Net into the MST reconstruction workflow significantly reduces the exposure time required to resolve high-Z materials, thereby improving the overall performance and practicality of the MST system.

IV. DISCUSSIONS

In this work, a comprehensive momentum-coupled muon scattering tomography (MST) simulation framework has been developed utilizing the Geant4 toolkit. Based on realistic laboratory configurations, we construct a detailed simulation system incorporating both Hp_{MRPC} and Ht_{MRPC} detectors, effectively coupling a ToF spectrometer with a traditional MST setup. The model fully accounts for muon energy loss during transportation, detector measurement uncertainties, and the extraction of muon momentum information, thereby forming an end-to-end simulation platform capable of providing practical guidance for future experimental implementations.

The primary imaging target considered in this study is the Fetter model: an intricate nuclear device. Both short-term displacement detection and non-destructive internal structure imaging are investigated. The results consistently show that integrating a ToF system into MST substantially improves imaging

quality and system performance and significantly reduces the exposure time required to resolve the internal high-Z components. Even though muons experience continuous energy loss and detectors introduce measurement uncertainties, appropriate momentum analysis and selection strategies still enable MST to extract maximal useful information. Furthermore, the application of a U-Net-based segmentation network demonstrates promising capability in identifying and enhancing high-Z structural features within MST images, indicating strong potential for real-world deployment.

Finally, this work clearly reveals that the Point-of-Closest-Approach (PoCA) algorithm, due to its inherent physical and geometrical limitations, performs poorly in reconstructing material boundaries: an issue particularly pronounced for complex multilayer structures such as the Fetter model. Future efforts should therefore focus on developing more advanced and better-suited reconstruction algorithms [**?**, **?**] to further enhance the performance and applicability of muon scattering tomography systems. Also, secondary particles in MST merit consideration [**?**].

V. ACKNOWLEDGMENTS

The work is supported by National Natural Science Foundation of China under Grant No. 11927901, 11420101004, 11461141011, 11275108, 11735009, U1832118. The work is also supported by the Ministry of Science and Technology of the People' s Republic of China under Grant No. 2020YFE0202001, 2018YFE0205200 and 2016YFA0400100.

VI. REFERENCES

[1] G. Bonomi, P. Checchia, M. D' Errico, D. Pagano, G. Saracino, Applications of cosmic-ray muons. Prog. Part. Nucl. Phys. 112, 103768 (2020). doi: 10.1016/j.ppnp.2020.103768

[2] S. Procureur, Muon imaging: Principles, technologies and applications. Nucl. Instrum. Methods Phys. Res. A 878, 169–179 (2018). doi: 10.1016/j.nima.2017.08.050

[3] R. He et al., Advances in nuclear detection and readout techniques, Nucl. Sci. Tech. 34(12), 205 (2023). doi: 10.1007/s41365-023-01346-5

[4] X.-Y. Pan et al., Experimental validation of material discrimination ability of muon scattering tomography at TUMUTY facility, Nucl. Sci. Tech. 30(8), 120 (2019). doi: 10.1007/s41365-019-0631-0

[5] S.-Y. Luo et al., Hybrid model for muon tomography and quantitative analysis of image quality, Nucl. Sci. Tech. 33(7), 81 (2022). doi: 10.1007/s41365-022-01005-5

[6] S.-T. Xiang and H. Liang, A time and charge measurement board for

muon tomography of high-Z materials, Nucl. Sci. Tech. 28(3), 40 (2017). doi: 10.1007/s41365-017-0182-1
[7] S. Barnes, A. Georgadze, A. Giammanco, M. Kiisk, V. A. Kudryavtsev, M. Lagrange, O. L. Pinto, Cosmic-ray tomography for border security. Instruments 7(1), 13 (2023). doi: 10.3390/instruments7010013
[8] Z. Zaher, H. Lay, T. Dorigo, A. Giammanco, V. Gulik, C. Hrytsiuk, V. A. Kudryavtsev, M. Lagrange, T. Metspalu, G. C. Strong et al., Optimization of a cosmic muon tomography scanner for cargo border control inspection. arXiv preprint arXiv:2507.10253 (2025). arXiv:2507.10253
[9] Z. Yifan, Z. Zhi, Z. Ming, W. Xuewu, Z. Ziran, Discrimination of drugs and explosives in cargo inspections by applying machine learning in muon tomography. High Power Laser and Particle Beams 30(8), 086002-1 (2018).
[10] G. Jonkmans, V. N. P. Anghel, C. Jewett, M. Thompson, Nuclear waste imaging and spent fuel verification by muon tomography. Ann. Nucl. Energy 53, 267–273 (2013). doi: 10.1016/j.anucene.2012.09.011
[11] A. Clarkson, S. Gardner, D. Ireland, R. Jebali, R. Kaiser, D. Mahon, M. Ryan, C. Shearer, G. Yang, Muon imaging applications for nuclear waste management and decommissioning. J. Adv. Instrum. Sci. 2022 (2022).
[12] S. Procureur, D. Attié, L. Gallego, H. Gomez, P. Gonzales, B. Lefèvre, M. Lehuraux, B. Lesage, I. Mandjavidze, P. Mas et al., 3D imaging of a nuclear reactor using muography measurements. Sci. Adv. 9(5), eabq8431 (2023). doi: 10.1126/sciadv.abq8431
[13] K. Takamatsu, H. Takegami, C. Ito, K. Suzuki, H. Ohnuma, R. Hino, T. Okumura, Cosmic-ray muon radiography for reactor core observation. Ann. Nucl. Energy 78, 166–175 (2015). doi: 10.1016/j.anucene.2014.11.015
[14] P. Martinez Ruiz del Arbol, A. Orio Alonso, C. Díez, P. Gómez García, Applications of muography to the industrial sector. J. Adv. Instrum. Sci. 2022 (2022).
[15] A. Sh. Georgadze, Rapid cargo verification with cosmic ray muon scattering and absorption tomography. J. Instrum. 19(10), P10033 (2024). doi: 10.1088/1748-0221/19/10/P10033
[16] Z. Chen, D. Liu, Y. Wang, D. Han, and H. Gong, Theoretical time cost to distinguish special nuclear materials in different scenarios through MPRC-ToF based muon scattering tomography. Nucl. Instrum. Methods Phys. Res. A 1057, 170557 (2025). doi: 10.1016/j.nima.2025.170557
[17] G. Yang, T. Clarkson, S. Gardner, D. Ireland, R. Kaiser, D. Mahon, R. A. Jebali, C. Shearer, M. Ryan, Novel muon imaging techniques. Philos. Trans. R. Soc. A 377(2137), 20180062 (2019). doi: 10.1098/rsta.2018.0062
[18] J. Bae, S. Chatzidakis, Momentum-dependent cosmic ray muon computed tomography using a fieldable muon spectrometer. Energies 15(7), 2666 (2022). doi: 10.3390/en15072666
[19] P. Yu, Z. Pan, J. Zhai, Y. Xu, L. Deng, Z. He, Z. Chen, Z. Kang, Y. Yu, X. Zhang et al., Improving Muon Scattering Tomography Performance With A Muon Momentum Measurement Scheme. arXiv preprint arXiv:2509.12800 (2025). arXiv:2509.12800
[20] J. Bae, R. Montgomery, S. Chatzidakis, Nuclear material accountancy

using momentum-informed muon scattering tomography. Ann. Nucl. Energy 197, 110240 (2024). doi: 10.1016/j.anucene.2024.110240
[21] F. Bury, M. Lagrange, Scattering-based machine learning algorithms for momentum estimation in muon tomography. Particles 8(2), 43 (2025). doi: 10.3390/particles8020043
[22] P. Aguiar et al., Geant4-GATE simulation of a large plastic scintillator for muon radiography, IEEE Trans. Nucl. Sci. 62(3), 1233–1238 (2015). doi: 10.1109/TNS.2015.2421015
[23] L. J. Schultz et al., Image reconstruction and material Z discrimination via cosmic ray muon radiography, Nucl. Instrum. Methods Phys. Res. A 519(3), 687–694 (2004). doi: 10.1016/j.nima.2003.11.019
[24] A. Blanco et al., Sealed (zero gas flow) resistive plate chambers, Eur. Phys. J. Plus 138(11), 1021 (2023). doi: 10.1140/epjp/s13360-023-04573-8
[25] E. C. Zeballos et al., A new type of resistive plate chamber: The multigap RPC, Nucl. Instrum. Methods Phys. Res. A 374(1), 132–135 (1996). doi: 10.1016/0168-9002(96)00349-8
[26] Y. Yu, D. Han, Y. Wang, B. Guo, F. Wang, X. Chen, P. Lyu, C. Shen, Q. Zhang, Y. Li, Study of high time resolution MRPC with the waveform digitizer system. J. Instrum. 15(01), C01049 (2020). doi: 10.1088/1748-0221/15/01/C01049
[27] W. J. Llope et al. (STAR Collaboration), Multigap RPCs in the STAR experiment at RHIC. Nucl. Instrum. Methods Phys. Res. A 661, S110–S113 (2012). doi: 10.1016/j.nima.2010.09.165
[28] S. Agostinelli et al., Geant4 —a simulation toolkit. Nucl. Instrum. Methods Phys. Res. A 506(3), 250–303 (2003). doi: 10.1016/S0168-9002(03)01368-8
[29] C. G. Wohl, R. N. Cahn, A. Rittenberg, T. G. Trippe, G. P. Yost, F. C. Porter, J. J. Hernandez, L. Montanet, R. E. Hendrick, R. L. Crawford, M. Roos, N. A. Törnqvist, G. Höhler, M. Aguilar-Benitez, T. Shimada, M. J. Losty, G. P. Gopal, Ch. Walck, R. E. Shrock, R. Frosch, L. D. Roper, W. P. Trower, B. Armstrong et al. (Particle Data Group), Review of particle properties, Rev. Mod. Phys. 56, S1 (1984).
[30] X. L. Chen et al., Development of Sealed MRPC with extremely low gas flow for muon tomography, J. Instrum. 15(03), C03012 (2020). doi: 10.1088/1748-0221/15/03/C03012
[31] O. Ronneberger, P. Fischer, and T. Brox, U-Net: Convolutional networks for biomedical image segmentation. In International Conference on Medical Image Computing and Computer-Assisted Intervention (MICCAI), pp. 234–241 (2015). Springer. doi: 10.1007/978-3-319-24574-4_{28}
[32] J. Wang, N. I. R. Ruhaiyem, and P. Fu, A comprehensive review of U-Net and its variants: Advances and applications in medical image segmentation, IET Image Processing 19(1), e70019 (2025). doi: 10.1049/ipr2.70019
[33] Y. A. Al-Naser and D. Tafti, CT Instrumentation and Physics. StatPearls, StatPearls Publishing, Treasure Island, FL (2025). Available online
[34] Y. Zhao et al., A cosmic ray muons tomography system with triangular bar plastic scintillator detectors and improved 3D image reconstruction algorithm: A simulation study, Nucl. Eng. Technol. 55(2), 681–689 (2023). doi:

10.1016/j.net.2022.08.027
[35] X. Cai et al., A new algorithm to improve imaging quality for muon tomography, Nucl. Instrum. Methods Phys. Res. A 1066, 169616 (2024). doi: 10.1016/j.nima.2023.169616
[36] X.-T. Ji et al., A novel 4D resolution imaging method for low and medium atomic number objects at the centimeter scale by coincidence detection technique of cosmic-ray muon and its secondary particles, Nucl. Sci. Tech. 33(1), 2 (2022). doi: 10.1007/s41365-021-00989-0